Steel and Composite Structures, *Vol. 36, No. 1* (*2020*) *1-16*
DOI: https://doi.org/10.12989/scs.2020.36.1.001

Vibration behavior of functionally graded sandwich beam with porous core and nanocomposite layers

Hua Si[1], Daoming Shen*[1], Jinhong Xia[1] and Vahid Tahouneh[2]

[1]*School of Civil Engineering & Architecture, Xinxiang university, Xinxiang, 453000, China*
[2]*Young Researchers and Elite Club, Islamshahr Branch, Islamic Azad University, Islamshahr, Iran*

(*Received January 13, 2020, Revised May 30, 2020, Accepted June 1, 2020*)

Abstract. This paper presents the influence of carbon nanotubes (CNTs) waviness, aspect ratio, internal pores and graphene platelets (GPLs) on the vibrational behavior of functionally graded nanocomposite sandwich beams resting on two-parameter elastic foundations. The distributions of CNTs are considered functionally graded (FG) or uniform along the thickness of upper and bottom layers of the sandwich beam and their mechanical properties are estimated by an extended rule of mixture. In this study, the classical theory concerning the mechanical efficiency of a matrix embedding finite length fibers has been modified by introducing the tube-to-tube random contact, which explicitly accounts for the progressive reduction of the tubes' effective aspect ratio as the filler content increases. The core of structure is porous and the internal pores and graphene platelets (GPLs) are distributed in the matrix of core either uniformly or non-uniformly according to three different patterns. The elastic properties of the nanocomposite are obtained by employing Halpin-Tsai micromechanics model. The equations of motion are derived based on Timoshenko beam theory and employing Hamilton's principle. The problem is modeled using a semi-analytical approach composed of generalized differential quadrature method (GDQM) and series solution adopted to solve the equations of motion. Detailed parametric studies are carried out to investigate carbon nanotubes (CNTs) waviness, CNT aspect ratio, porosity coefficient, porosity distribution, graphene platelets (GPLs) distribution, Winkler foundation modulus, shear elastic foundation modulus and geometrical conditions on the vibrational behavior of the sandwich structure.

Keywords: CNTs waviness and aspect ratio; sandwich beams; vibration; rule of mixture; two-parameter elastic foundations; functionally graded materials; porous core; Halpin-Tsai micromechanics model

1. Introduction

Normally, Functionally graded materials (FGMs) are heterogeneous materials in which the elastic and thermal properties change from one surface to the other, gradually and continuously. The material is constructed by smoothly changing the volume fraction of its constituent materials. FGMs offer great promise in applications where the operating conditions are severe, including spacecraft heat shields, heat exchanger tubes, plasma facings for fusion reactors, engine components, and high-power electrical contacts or even magnets. For example, in a conventional thermal barrier coating for high-temperature applications, a discrete layer of ceramic material is bonded to a metallic structure. However, the abrupt transition in material properties across the interface between distinct materials can cause large interlaminar stresses and lead to plastic deformation or cracking (Finot and Suresh 1996). These adverse effects can be alleviated by functionally grading the material to have a smooth spatial variation of material composition. The concept of FGMs was first introduced in Japan in 1984. Since then it has gained considerable attention (Koizumi 1993).

A lot of different applications of FGMs can be found in (Zhu and Meng 1995). Mahmoud *et al.* (2011) investigated free vibration analysis of a non-uniform column resting on an elastic foundation and subjected to follower force. Smith and Herrmann (1972) introduced a stability of a cantilevered beam on an elastic foundation subjected to a follower force at its free end. He found that the critical load for flutter is independent of the foundation modulus which characterizes the Winkler-type embedding. Sundararajan (1974) presented stability of columns on Winkler type elastic foundations subjected to stationary forces (conservative or non-conservative). Various cases were discussed and a theorem on the influence of the foundation on the critical load was derived. Hauger and Vetter (1976) discussed the influence of an elastic foundation on the stability of a tangentially loaded column. Celep (1980) presented the stability analysis of a beam on an elastic foundation subjected to a nonconservative load. Based on the Lagrange interpolation Chan (Quan and Chan 1989) provided explicit formulations to compute the weighting coefficients of the DQ discretization of the first and second order derivatives. Application of DQM to flexural vibration analysis of a geometrically nonlinear beam was introduced by Yusheng Feng and Bert (1992). There are many types of grid distributions such as; uniform space grid distribution. It was introduced by Wang and Bert (1993) as a new approach

*Corresponding author, Ph.D.
E-mail: daiomingshen@126.com
**Corresponding author, Ph.D.
E-mail: vahid.th1982@gmail.com

Copyright © 2020 Techno-Press, Ltd.

ISSN: 1229-9367 (Print), 1598-6233 (Online)

in applying DQ to free vibration analysis of a beam and plates. Bert and Malik (1996) indicated an important fact that the preferred type of grid points changes with the problem of interest; and recommended to use Chebyshev-Gauss-Lobatto grid distributions for structural mechanics computation. Lee and Yang (1994) discussed the influence of a Winkler elastic foundation and the slenderness ratio on the non-conservative instability of cantilever non-uniform beams subjected to an end concentrated follower force. Du *et al.* (1996) applied the DQM to the buckling analysis of columns and plates. The numerical results obtained were compared with those from existing literature and achieved high accuracy. Also there are many types of implementation of boundary conditions such as δ-type a small distance δ from the boundary. It was developed in the DQM to apply more than one boundary condition at discretized point; these results often based on value of δ and may be get ill-conditioned matrices. The clamped and simply supported boundary conditions using generalized DQ were introduced by Shu and Du (1997a). This approach directly substitutes the boundary conditions into the governing equations, abbreviated as SBCGE. It was used to overcome the drawbacks of δ-type. Also Shu and Du (1997b) presented an implementation of the general boundary conditions in the free vibration analysis of rectangular plates which directly couples the boundary conditions with the governing equations, abbreviated as CBCGE. As shown in the book of Shu (2000) the DQ is a global method, which is equivalent to the highest-order finite difference scheme. As compared to the low order finite difference schemes and finite element methods, the DQM can obtain very accurate numerical results by using a considerably small number of grid points. Consequently, it requires less computational effort and virtual storage. In general, the DQM uses a non-uniform mesh for numerical discretization. Karami *et al.* (2003) discussed that the differential quadrature element method (DQEM) could be employed as an accurate method for practical beam applications. The DQEM was applied to a non-uniform or discontinuous cross section beam and a beam subjected to heavy concentrated masses resting on elastic foundation in comparison with the finite element method. Ebrahimi *et al.* (2019) proposed a new gusset plate passing through the HSS columns and beams, named as through gusset plate to study the force transfer mechanism in such gusset plates of SCBFs compared to the case with conventional gusset plates. Nguyen *et al.* (2019) investigate the static behavior of a novel RCS beam-column exterior joint. The studied joint detail is a through-column type in which an H steel profile totally embedded inside RC column is directly welded to the steel beam. Wang and Sun (2019) investigate on seismic behavior of out-of-code Q690 circular high-strength concrete-filled thin-walled steel tubular (HCFTST) columns made up of high-strength (HS) steel tubes (yield strength $f_y \geq 690$ MPa). Six shear-critical square tubed steel reinforced concrete (TSRC) columns using the high-strength concrete ($f_{cu,150} = 86.6$ MPa) were tested under constant axial and lateral cyclic loads (Li *et al.* 2019). Song *et al.* (2019) present a preliminary numerical study on stainless steel-concrete composite beam-to-column joints with bolted flush endplates. In order to ensure a consistent corrosion resistance within the whole structural system, all structural steel components were designed with austenitic stainless steel, including beams, columns, endplates, bolts, reinforcing bars and shear connectors. Lai *et al.* (2019) report additional test data, analytical and numerical studies leading to a new design method to predict the ultimate resistance of composite columns made of high strength steel and high strength concrete. Bambaeechee (2019) investigates free vibration of AFG and uniform beams with general elastic supports. An efficient and free of shear locking finite element model is developed and employed to study free vibration of tapered bidirectional functionally graded material (BFGM) beams by Nguyen and Tran (2018). Investigation on the thermal buckling resistance of simply supported FGM beams having parabolic-concave thickness variation and temperature dependent material properties is presented by Arioui *et al.* (2018). Hadji *et al.* (2014) study static and free vibration of functionally graded beams via a higher order shear deformation beam theory. Mirjavadi *et al.* (2017) investigate the thermo-mechanical vibration behavior of two dimensional functionally graded (2D-FG) porous nanobeam. Shafiei and Setoodeh (2017) study the nonlinear free vibration and post-buckling of functionally graded carbon nanotube reinforced composite (FG-CNTRC) beams resting on a nonlinear elastic foundation. Yaghoobi *et al.* (2014) investigate nonlinear vibration and post-buckling of beams made of functionally graded materials (FGMs) resting on nonlinear elastic foundation subjected to thermo-mechanical loading. Marin *et al.* (2013) studied nonsimple material problems using Lagrange's identity. They proved the uniqueness theorem and some continuous dependence theorems without recourse to any any energy conservation on the thermoelastic coefficients. Marin (2010) used Lagrange identity approach for microstretch thermoelastic materials. Marin (2010) considered a right cylinder composed of a physically dipolar thermoelastic material for wich one plane end was subjected to an excitation which was harmonic in time. In some other papers, researchers studies different problems relating to the void and porosity (Marin and Nicaise 2016, Marin *et al.* 2016, Marin *et al.* 2017). Sharma *et al.* (2005a, 2005b) integrated an analytical approach with the Chebyshev polynomials technique to study the buckling and free vibration of isotropic and laminated composite sector plates based on the first-order shear deformation theory. Liu and Wang (2015) studied Thermal vibration of a single-walled carbon nanotube predicted by semiquantum molecular dynamics. Zhang and Wang (2018) investigated the nonlinear thermal vibrational behavior of single-layered BP (SLBP) via a nonlinear orthotropic plate model (OPM) and molecular dynamics (MD) simulations. Xu *et al.* (2016) studied the vibration of double-layered graphene sheets (DLGS) using A nonlocal Kirchhoff plate model with the van der Waals (vdW)

interactions. Ahmed Houari *et al.* (2018) presented a closed-form solutions for exact critical buckling loads of nonlocal strain gradient functionally graded beams. Chen *et al.* (2017) investigated vibration and stability of initially stressed sandwich plates with FGM face sheets. Barka *et al.* (2016) studied thermal post-buckling behavior of imperfect temperature-dependent FG structures. Bouguenina *et al.* (2015) studied FG plates with variable thickness subjected to thermal buckling. Park *et al.* (2016) used modified couple stress based third-order shear deformation theory for dynamic analysis of sigmoid functionally graded materials (S-FGM) plates. Wu and Liu (2016) developed a state space differential reproducing kernel (DRK) method in order to study 3D analysis of FG circular plates. Arefi (2015) suggested an analytical solution of a curved beam with different shapes made of functionally graded materials (FGMs). Bennai *et al.* (2015) developed a new refined hyperbolic shear and normal deformation beam theory to study the free vibration and buckling of functionally graded (FG) sandwich beams under various boundary conditions. Bouchafa *et al.* (2015) used refined hyperbolic shear deformation theory (RHSDT) for the thermoelastic bending analysis of functionally graded sandwich plates. Tornabene *et al.* (2019) investigated free vibration analysis of arches and beams made of composite materials via a higher-order mathematical formulation. Tornabene *et al.* (2017) studied free vibration analysis of composite sandwich plates and doubly curved shells with variable stiffness. The reinforcing fibers were located in the external skins of the sandwich structures according to curved paths. Tornabene *et al.* (2018) studied free vibration of laminated nanocomposite plates and shells using first-order shear deformation theory and the Generalized Differential Quadrature (GDQ) method. Each layer of the laminate was modelled as a three-phase composite. A survey of several methods under the heading of strong formulation finite element method (SFEM) was presented by Tornabene *et al.* (2015). Tahouneh (2016) presented a 3-D elasticity solution for free vibration analysis of continuously graded carbon nanotube-reinforced (CGCNTR) rectangular plates resting on two-parameter elastic foundations. The volume fractions of oriented, straight single-walled carbon nanotubes (SWCNTs) were assumed to be graded in the thickness direction. Moradi-Dastjerdi and Momeni-Khabisi (2016) studied Free and forced vibration of plates reinforced by wavy carbon nanotube (CNT). The plates were resting on Winkler-Pasternak elastic foundation and subjected to periodic or impact loading.

Nowadays, the use of carbon nanotubes in polymer/carbon nanotube composites has attracted wide attention (Wagner *et al*. 1997). A high aspect ratio, low weight of CNTs and their extraordinary mechanical properties (strength and flexibility) provide the ultimate reinforcement for the next generation of extremely lightweight but highly elastic and very strong advanced composite materials. On the other hand, by using of the polymer/CNT composites in advanced composite materials, we can achieve structures with low weight, high strength and high stiffness in many structures of civil, mechanical and space engineering.

Many researchers have reported that mechanical properties of polymeric matrices can be drastically increased (Montazeri *et al.* 2010, Yeh *et al.* 2006) by adding a few weight percent (wt%) MWCNTs. Montazeri *et al.* (2010) showed that modified Halpin-Tsai equation with exponential Aspect ratio can be used to model the experimental result of MWNT composite samples. They also demonstrated that reduction in Aspect ratio (L/d) and nanotube length cause a decrease in aggregation and Above 1.5 wt%, nanotubes agglomerate causing a reduction in Young's modulus values. Thus, it is important to determine the effect Aspect ratio and arrangement of CNTs on the effective properties of carbon nanotube-reinforced composite (CNTRC). Yeh *et al.* (2006) used the Halpin-Tsai equation to shows the effect of MWNT shape factor (L/d) on the mechanical properties. They showed that the mechanical properties of nanocomposite samples with the higher shape factor (L/d) values were better than the ones with the lower shape factor. The reinforcement effect of MWCNTs with different aspect ratio in an epoxy matrix has been carried out by Martone *et al.* (2011). They showed that progressive reduction of the tubes effective aspect ratio occurs because of the increasing connectedness between tubes upon an increase in their concentration. Also they investigated on the effect of nanotube curvature on the average contacts number between tubes by means of the waviness that accounts for the deviation from the straight particles assumption. The material properties of FG-CNTR can be evaluated through a micromechanical model in which CNT efficiency parameters are estimated by matching the elastic moduli of the CNTR observed from the molecular dynamics (MD) simulation with that of numerical results obtained from the rule of mixture (Shen 2009).

Analysis of FG-CNTR plates and beams were first presented by Shen (2009) in which he studied the nonlinear bending behavior of FG-CNTR plates in thermal environment. He concluded that the load bending moment curves of the plate could be significantly increased as a result of functionally graded CNT reinforcements. Shen and Zhang (2010) presented thermal buckling and post buckling behavior of functionally graded nanocomposite plates reinforced by single-walled carbon nanotubes (SWCNTs). The temperature-dependent material properties of SWCNTs were obtained from MD simulations. In comparison with research works on the free vibration or buckling analyses of FG structures, only a few references can be found that consider the effect of waviness and aspect ratio on the free vibrational behavior of panels with four edges simply supported (Moradi-Dastjerdi, Foroutan, and Pourasghar 2013). Moradi-Dastjerdi, Foroutan, and Pourasghar (2013) investigated the effects of CNT waviness on the dynamic behavior of FG-CNTR cylinder under impact load.

Despite the aforementioned extensive research on the free vibration analysis of structures resting on elastic foundations, to the authors' best knowledge, still very little work has been done for vibration analysis of FG-CNTR

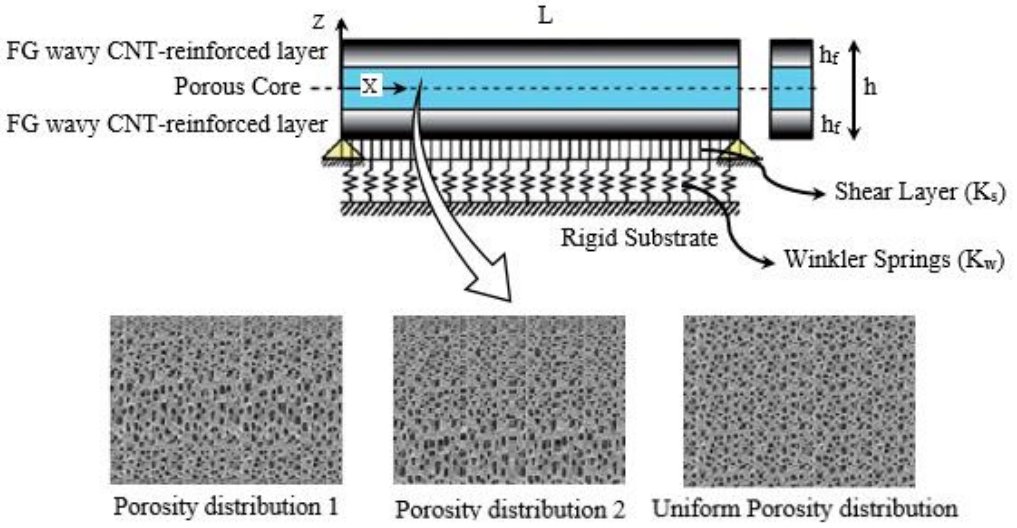

Fig. 1 Geometry of FG sandwich beam with porous core and nanocomposite layers.

structures and considering the effect of waviness and aspect ratio on their vibrational response. The aim of this study is to fill this apparent gap in this area by investigating the influence of carbon nanotubes (CNTs) waviness, aspect ratio, internal pores and graphene platelets (GPLs) on the vibrational behavior of functionally graded nanocomposite sandwich beams resting on two-parameter elastic foundations. The distributions of CNTs are considered functionally graded (FG) or uniform along the thickness of upper and bottom layers of the sandwich beam and their mechanical properties are estimated by an extended rule of mixture. In this study, the classical theory concerning the mechanical efficiency of a matrix embedding finite length fibers has been modified by introducing the tube-to-tube random contact, which explicitly accounts for the progressive reduction of the tubes' effective aspect ratio as the filler content increases. The core of structure is porous and the internal pores and graphene platelets (GPLs) are distributed in the matrix of core either uniformly or non-uniformly according to three different patterns.

2. Problem description

Consider an FG sandwich beam resting on Pasternak foundations as shown in Fig. 1. It is assumed that the total thickness of beam is "h", the thickness of faces is "h_f" and the length of structure assumed to be "L". The FG wavy CNT-reinforced faces are made from a mixture of wavy SWCNTs and isotropic matrix and the core of structure is considered to be porous as depicted in Fig. 1.

3. Carbon nanotubes (CNTs) waviness and Porosity

3.1 Mechanical properties of the wavy SWCNT reinforcement

The wavy SWCNT reinforcement is either uniformly distributed (UD) or functionally graded in the faces of beam. Employing the extended rule of mixture the effective elastic properties of the CNTR beam can be expressed as follows (Shen 2009)

$$E_{11} = \eta_1 V_{CNT} E_{11,\eta^*}^{CNT} + V_m E^m \tag{1}$$

$$\frac{\eta_2}{E_{22}} = \frac{V_{CNT}}{E_{22,\eta^*}^{CNT}} + \frac{V_m}{E^m} \tag{2}$$

$$\frac{\eta_3}{G_{12}} = \frac{V_{CNT}}{G_{12,\eta^*}^{CNT}} + \frac{V_m}{G^m} \tag{3}$$

$$\upsilon_{12} = V_{CNT} \upsilon_{12}^{CNT} + V_m \upsilon^m \tag{4}$$

$$\rho = V_{CNT} \rho^{CNT} + V_m \rho^m \tag{5}$$

where E_{11,η^*}^{CNT}, E_{22,η^*}^{CNT}, G_{12,η^*}^{CNT} υ_{12}^{CNT} and ρ^{CNT} denote effective Young's moduli, effective shear modulus, Poisson's ratios and density of the CNT, respectively. E^m, G^m, υ^m and ρ^m are the corresponding properties of the isotropic matrix. η_j (j=1,2,3) are the CNT efficiency parameters accounting for the scale-dependent material properties evaluated by comparing the effective material properties obtained from MD simulations and that of numerical results obtained from the rule of mixture in (Shen 2009).

V_{CNT} and V_m are the CNT and matrix volume fractions related by

$$V_{CNT} + V_m = 1 \tag{6}$$

The effective Young's moduli and shear modulus of wavy CNT are introduced as follows (Martone *et al.* 2011)

$$E_{ii,\eta^*}^{CNT} = \eta^* E_{ii}^{CNT}, i = 1,2$$
$$G_{12,\eta^*}^{CNT} = \eta^* G_{12}^{CNT} \quad (7)$$

where

$$\eta^* = 1 - \frac{\tanh(K.AR/(1+<c>))}{K.AR/(1+<c>)}$$
$$K = \sqrt{\frac{-2}{1+\upsilon_m} / \left(\frac{E_{11}^{CNT}}{E_{11}^{m}} \ln V_{CNT}\right)} \quad (8)$$

The efficiency parameter, η^* is considered to account the CNT aspect ratio and waviness (Martone *et al.* 2011). $<c>$ is the average number of contacts for CNTs depends on their aspect ratio defined as

$$<c> = wV_{CNT} + \left(4 + \frac{3AR^2}{3AR+2}\right) \quad (9)$$

where the waviness, *w*, has been introduced for accounting the CNT's curvature within the CNTR structure (Martone *et al.* 2011). Introducing this parameter, the excluded volume due to the curvature of CNTs has been considered. The accuracy of this method has been investigated by (Moradi-Dastjerdi *et al.* 2013). The variation of CNT distribution through the face thickness can be stated as

$$FG-V: \begin{cases} V_{CNT} = 2\left(1+\frac{z-h/2}{h_f}\right)V_{CNT}^*, for \ \ 0.2 < z/h < 0.5 \\ V_{CNT} = 2\left(1+\frac{-z-h/2}{h_f}\right)V_{CNT}^*, for \ \ -0.5 < z/h < -0.2 \end{cases},$$

$$FG-\Lambda: \begin{cases} V_{CNT} = -2\left(\frac{2z-h}{2h_f}\right)V_{CNT}^*, for \ \ 0.2 < z/h < 0.5 \\ V_{CNT} = 2\left(\frac{2z+h}{2h_f}\right)V_{CNT}^*, for \ \ -0.5 < z/h < -0.2 \end{cases},$$

$$FG-X: \begin{cases} V_{CNT} = 2\left(1+\frac{2}{h_f}(z-h/2)\right)V_{CNT}^*, for \ \ 0.35 < z/h < 0.5 \\ V_{CNT} = 2\left(-1-\frac{2}{h_f}(z-h/2)\right)V_{CNT}^*, for \ \ 0.2 < z/h < 0.35 \\ V_{CNT} = 2\left(-1-\frac{2}{h_f}(-z-h/2)\right)V_{CNT}^*, for \ \ -0.35 < z/h < -0.2 \\ V_{CNT} = 2\left(1+\frac{2}{h_f}(-z-h/2)\right)V_{CNT}^*, for \ \ -0.5 < z/h < -0.35 \end{cases}, \quad (10)$$

$$FG-\Diamond: \begin{cases} V_{CNT} = \frac{4}{h_f}(-z+h/2)V_{CNT}^*, for \ \ 0.35 < z/h < 0.5 \\ V_{CNT} = \frac{4}{h_f}(z-h/2+h_f)V_{CNT}^*, for \ \ 0.2 < z/h < 0.35 \\ V_{CNT} = \frac{4}{h_f}(-z-h/2+h_f)V_{CNT}^*, for \ \ -0.35 < z/h < -0.2 \\ V_{CNT} = \frac{4}{h_f}(z+h/2)V_{CNT}^*, for \ \ -0.5 < z/h < -0.35 \end{cases},$$

$$UD: \begin{cases} V_{CNT} = V_{CNT}^*, for \ \ 0.2 < z/h < 0.5 \\ V_{CNT} = V_{CNT}^*, for \ \ -0.5 < z/h < -0.2 \end{cases}$$

Table 1 Properties of the (10,10) SWCNT and the polymer matrix (Shen and Zhang 2010).

SWCNT	Polymer matrix
$E_{11}^{CNT} = 5.6466(TPa), E_{22}^{CNT} = 7.0800(TPa),$	$E^m = 2.1(GPa)$
$G_{12}^{CNT} = 1.9447(TPa), \rho^{CNT} = 1400(Kg/m^3)$	$\rho^m = 1150(Kg/m^3)$
$\upsilon_{12} = 0.175$	$\upsilon^m = 034$

Table 2 CNT efficiency parameters for different values of volume fractions (Shen and Zhang 2010)

V_{CNT}^*	η_1	η_2	η_3
0.12	0.137	1.022	0.715
0.17	0.142	1.626	1.138
0.28	0.141	1.585	1.109

where

$$V_{CNT}^* = \frac{w_{CNT}}{w_{CNT} + (\rho^{CNT}/\rho^m)(1-w_{CNT})} \quad (11)$$

V_{CNT}^* is the CNT volume fraction and w_{CNT} is the mass fraction of CNTs. Poly methyl methacrylate, referred to as PMMA and (10,10) SWCNTs are selected as the matrix and the reinforcement materials, respectively. The material properties for the constituent materials are listed in Table 1 (Shen and Zhang 2010).

Values of CNT efficiency parameters, $\eta_i (i = 1,2,3)$, for different CNT volume fractions are presented in Table 2 to capture the scale difference between micro and nano levels. It should be noted that $\eta_3 = 0.7\eta_2, G_{13} = G_{12}$ and $G_{23} = 1.2G_{12}$ (Shen and Zhang 2010).

3.2 Mechanical properties of a porous structure with different types of porosity distributions

Three different GPL dispersion patterns, denoted by A, B, and C, are considered for each porosity distribution (Fig. 2). The GPL volume content V_{GPL} is assumed to vary along the thickness smoothly with its peak values (S_{ij}, i,j=1, 2, 3) being determined based on the specific porosity distribution.

To facilitate a direct and meaningful comparison, the total amount of GPLs is kept the same for three different GPL distribution patterns. This leads to $s_{1i} \neq s_{2i} \neq s_{3i}$ (i=1, 2, 3).

The mechanical properties of a porous structure with different types of porosity distributions can be expressed by

$$E(z) = E_1(1 - e_0\lambda(z)) \quad (12)$$

$$G(z) = E(z)/2(1+\upsilon(z)) \quad (13)$$

$$\rho(z) = \rho_1(1 - e_m\lambda(z)) \quad (14)$$

in which, for symmetric porosity distribution

$$\lambda(z) = \cos(\pi z/h) \quad (15)$$

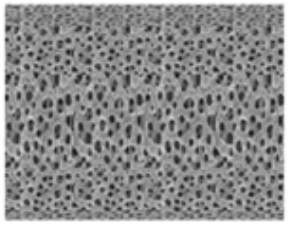

(A) Non-uniform porosity distribution 1 with three GPL dispersion patterns.

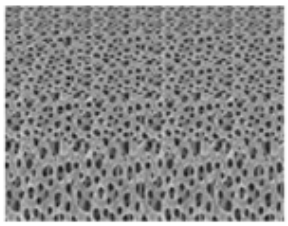

(B) Non-uniform porosity distribution 2 with three GPL dispersion patterns.

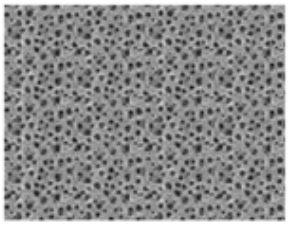

(C) Uniform porosity distribution with three GPL dispersion patterns.

Fig. 2 Porosity distribution and GPL dispersion patterns

for asymmetric porosity distribution

$$\lambda(z)=\cos(\pi z/2h+\pi/4) \tag{16}$$

and for uniform porosity distribution

$$\lambda(z)=\lambda \tag{17}$$

where E_1, G_1, and ρ_1 are the maximum values of elasticity moduli, shear moduli and mass density.

Also, e_0 and e_m are the coefficients of porosity and mass density, respectively, defined by (Kitipornchai *et al*. 2017)

$$\begin{aligned} e_0 &= 1-\frac{E_2}{E_1}=1-\frac{G_2}{G_1} \\ e_m &= \frac{1.121(1-\sqrt[2.3]{1-e_0\lambda(z)})}{\lambda(z)} \end{aligned} \tag{18}$$

Also based on the closed-cell graphene-reinforcement scheme, Poisson's ratio (z) can be expressed by (Kitipornchai *et al.* 2017)

$$\upsilon(z)=0.221\tilde{p}+\upsilon_1(0.342\tilde{p}^2-1.21\tilde{p}+1) \tag{19}$$

In which $\boldsymbol{\upsilon}_1$ is the Poisson's ratio of pure matrix materials without pores and

$$\tilde{p}=1.121(1-\sqrt[2.3]{1-e_0\lambda(z)}) \tag{20}$$

Also, λ(z) for uniform porosity distribution can be expressed by

$$\lambda=\frac{1}{e_0}-\frac{1}{e_0}\left(\frac{\tilde{M}/h+0.121}{1.121}\right)^{2.3} \tag{21}$$

In which

$$\tilde{M}=\int_{-h/2}^{h/2}(1-\tilde{p})dz \tag{22}$$

According to the distribution patterns depicted in Fig. 2, the volume fraction of GPLs can be written as (i=1,2,3)

$$V_{GPL}=\begin{cases} S_{i1}\left[1-\cos(\pi z/h\right], \text{Pattern A} \\ S_{i2}\left[1-\cos(\pi z/2h+\pi/4\right], \text{Pattern B} \\ S_{i3}, \text{Pattern C} \end{cases} \tag{23}$$

The relation between the volume fraction of GPLs and their weight fraction W_{GPL} can be expressed by

$$\frac{W_{GPL}}{W_{GPL}+\frac{\rho_{GPL}}{\rho_M}-\frac{\rho_{GPL}}{\rho_M}W_{GPL}}\int_{-h/2}^{h/2}(1-e_m\lambda(z))dz = \int_{-h/2}^{h/2}V_{GPL}(1-e_m\lambda(z))dz \tag{24}$$

In which ρ_{GPL} and ρ_M are mass density of GPL and metal matrix, respectively. Based on Halpin-Tsai micromechanical model, it is possible to obtain material properties of GPL-reinforced metal matrix structures

$$E_1=\frac{3}{8}\left(\frac{1+\xi_L^{GPL}\eta_L^{GPL}V_{GPL}}{1-\eta_L^{GPL}V_{GPL}}\right)E_M+\frac{5}{8}\left(\frac{1+\xi_W^{GPL}\eta_W^{GPL}V_{GPL}}{1-\eta_W^{GPL}V_{GPL}}\right)E_M \tag{25}$$

in which E_m is Young's modulus of the metal and

$$\xi_L^{GPL}=2l_{GPL}/t_{GPL},\ \eta_L^{GPL}=\frac{(E_{GPL}/E_M)-1}{(E_{GPL}/E_M)+\xi_L^{GPL}},\quad \xi_W^{GPL}=2w_{GPL}/t_{GPL},\ \eta_W^{GPL}=\frac{(E_{GPL}/E_M)-1}{(E_{GPL}/E_M)+\xi_W^{GPL}} \tag{26}$$

w_{GPL}, l_{GPL} and t_{GPL} denote GPLs' average width, length, and thickness, respectively. Finally, Poisson's ratio of GPL-reinforced metal matrix implementing rule of mixture can be expressed by

$$\upsilon_1=\upsilon_{GPL}V_{GPL}+\upsilon_M V_M \tag{27}$$

where V_M is the volume fraction of metal matrix (V_M= 1−V_{GPL}).

4. Equations of motion

The sandwich beam is assumed to be rested on the two-parameter elastic (Pasternak) foundation whose supporting action is described by

$$P=K_w w-K_s\frac{\partial^2 w}{\partial x^2} \tag{28}$$

where P is the foundation reaction per unit area, *w* is the transverse deflection of the beam, and K_w and K_s are Winkler and shearing layer elastic coefficients of the foundation. Based on Timoshenko beam theory, the displacements of any point in the beam along the x- and z-axes, represented by U(x, z, t) and W(x, z, t), respectively, are as follows

$$U(x,z,t)=u_0(x,t)+z\psi(x,t),\quad W(x,z,t)=w_0(x,t) \tag{29}$$

in which u_0 and w_0 represent the components of displacement at z=0, $\boldsymbol{\psi}$ is the section normal vector rotation about the y-axis, and t is time. The linear normal strain ε_x and shear strain γ_{xz} are associated with the displacements as

$$\varepsilon_x=\frac{\partial u_0}{\partial x}+z\frac{\partial \psi}{\partial x},\ \gamma_{xz}=\frac{\partial w_0}{\partial x}+\psi \tag{30}$$

Using the linear elastic constitutive law, the normal stress σ_x and shear stress τ_{xz} are given by

$$\sigma_x(z)=Q_{11}(z)\varepsilon_x,\quad \tau_{xz}(z)=Q_{55}(z)\gamma_{zx} \tag{31}$$

In which

$$Q_{11}(z)=\frac{E(z)}{1-\upsilon^2},Q_{55}(z)=\frac{E(z)}{2(1+\upsilon)} \tag{32}$$

Employing Hamilton's principle, the equations of motion and the related boundary conditions can be derived. It is formulated as

$$\delta\int_0^t(T-\prod+\gamma_p)dt=0 \tag{33}$$

where δ, T, and Π denote variational symbol, kinetic energy of the beam, and potential energy composed of strain energy the beam together with the elastic potential energy of the foundation, respectively. It is worth noting that γ_p is the work done by external force that is zero for free vibration analysis.

$$T=\frac{b}{2}\int_0^L\int_{-h/2}^{h/2}\rho(z)\left\{(\frac{\partial U}{\partial t})^2+(\frac{\partial W}{\partial t})^2\right\}dzdx,$$
$$\prod=\frac{b}{2}\int_0^L\int_{-h/2}^{h/2}(\sigma_x\varepsilon_x+k^*\tau_{xz}\gamma_{xz})dzdx+\frac{b}{2}\int_0^L\left(K_w W^2 K_s(\frac{\partial W}{\partial x})^2\right)dx \tag{34}$$

In this study, the shear correction factor k^*=5/6 is used. Substituting equation (34) into equation (33) and integrating through the thickness of beam and then setting the coefficients of δu, δw_0, and $\delta\boldsymbol{\psi}$ to zero lead to the equations of motion as

$$\delta u_0:\frac{\partial N_x}{\partial x}=I_1\frac{\partial^2 u_0}{\partial t^2}+I_2\frac{\partial^2\psi}{\partial t^2} \tag{35}$$

$$\delta w_0:\frac{\partial Q_x}{\partial x}-K_f w_0+K_s\frac{\partial^2 w_0}{\partial x^2}=I_1\frac{\partial^2 w_0}{\partial t^2} \tag{36}$$

$$\delta\psi:\frac{\partial M_x}{\partial x}-Q_x=I_2\frac{\partial^2 u_0}{\partial t^2}+I_3\frac{\partial^2\psi}{\partial t^2} \tag{37}$$

where N_x, M_x, and Q_x are axial force, bending moment, and shear force, which can be defined as

$$\begin{Bmatrix}N_x\\M_x\\Q_x\end{Bmatrix}=\int_{-h/2}^{h/2}\begin{Bmatrix}\sigma_{xx}\\z\sigma_{xx}\\\tau_{xz}\end{Bmatrix}dz \tag{38}$$

By combining Eqs. (30)-(32) and Eq. (37), we have

$$N_x=A_{11}\frac{\partial u_0}{\partial x}+B_{11}\frac{\partial\psi}{\partial x},M_x=B_{11}\frac{\partial u_0}{\partial x}+D_{11}\frac{\partial\psi}{\partial x},\quad Q_x=k^*A_{55}(\frac{\partial w_0}{\partial x}+\psi) \tag{39}$$

The stiffness components A_{11}, B_{11}, D_{11}, A_{55} and the inertia-related terms I_1, I_2, I_3 of the beam are defined as

$$(A_{11},B_{11},D_{11})=\int_{-h/2}^{h/2}Q_{11}(z)(1,z,z^2)dz,\quad A_{55}=\int_{-h/2}^{h/2}Q_{55}(z)dz,\quad (I_1,I_2,I_3)=\int_{-h/2}^{h/2}\rho(z)(1,z,z^2)dz \tag{40}$$

Substituting Eq. (39) into Eqs. (35)-(37) leads to the following equations

$$A_{11}\frac{\partial^2 u_0}{\partial x^2}+B_{11}\frac{\partial^2\psi}{\partial x^2}=I_1\frac{\partial^2 u_0}{\partial t^2}+I_2\frac{\partial^2\psi}{\partial t^2} \tag{41}$$

$$k^* A_{55}(\frac{\partial^2 w_0}{\partial x^2}+\frac{\partial \psi}{\partial x})-K_w w_0+K_s\frac{\partial^2 w_0}{\partial x^2}=I_1\frac{\partial^2 w_0}{\partial t^2} \quad (42)$$

$$B_{11}\frac{\partial^2 u_0}{\partial x^2}+D_{11}\frac{\partial^2 \psi}{\partial x^2}-k^* A_{55}(\frac{\partial w_0}{\partial x}+\psi)=I_2\frac{\partial^2 u_0}{\partial t^2}+I_3\frac{\partial^2 \psi}{\partial t^2} \quad (43)$$

Different boundary conditions of the beams such as Clamped-Hinged (C-H), Clamped-Clamped (C-C), and Clamped-Free (C-F) are considered. These conditions can be described as

Clamped (C): $u_0=w_0=\psi=0$
Hinged (H): $u_0=w_0=M_x=0$ (44)
Free (F): $N_x=Q_x=M_x=0$

For simplicity and generality the following dimensionless quantities are introduced

$$\begin{aligned}
&\xi=\frac{x}{L},(\bar{U},\bar{W})=\frac{(u_0,w_0)}{h},\\
&(\bar{I}_1,\bar{I}_2,\bar{I}_3)=(\frac{I_1}{I_{10}},\frac{I_2}{I_{10}h},\frac{I_3}{I_{10}h^2}),\bar{\eta}=\frac{L}{h},\bar{\psi}=\psi\\
&(a_{11},a_{55},b_{11},d_{11})=(\frac{A_{11}}{A_{110}},\frac{A_{55}}{A_{110}},\frac{B_{11}}{A_{110}h},\frac{D_{11}}{A_{110}h^2}),\\
&\tau=\frac{t}{L}\sqrt{\frac{A_{110}}{I_{10}}},k_w=\frac{K_w L^2}{A_{110}},k_s=\frac{K_s}{A_{110}}
\end{aligned} \quad (45)$$

in which A_{110} and I_{10} are the values of A_{11} and I_1 of a homogeneous beam made from pure matrix material. Thus, Eqs. (41)-(43) can be transformed into the following dimensionless forms

$$a_{11}\frac{\partial^2 \bar{U}}{\partial \xi^2}+b_{11}\frac{\partial^2 \bar{\psi}}{\partial \xi^2}=\bar{I}_1\frac{\partial^2 \bar{U}}{\partial \tau^2}+\bar{I}_2\frac{\partial^2 \bar{\psi}}{\partial \tau^2} \quad (46)$$

$$k^* a_{55}(\frac{\partial^2 \bar{W}}{\partial \xi^2}+\eta\frac{\partial \bar{\psi}}{\partial \xi})-k_w\bar{W}+k_s\frac{\partial^2 \bar{W}}{\partial \xi^2}=\bar{I}_1\frac{\partial^2 \bar{W}}{\partial \tau^2} \quad (47)$$

$$b_{11}\frac{\partial^2 \bar{U}}{\partial \xi^2}+d_{11}\frac{\partial^2 \bar{\psi}}{\partial \xi^2})-k^*\bar{\eta}a_{55}(\frac{\partial \bar{W}}{\partial \xi}+\bar{\eta}\bar{\psi})=\bar{I}_2\frac{\partial^2 \bar{U}}{\partial \tau^2}+\bar{I}_3\frac{\partial^2 \bar{\psi}}{\partial \tau^2} \quad (48)$$

5. GDQ approach

Here, GDQ technique is used to solve the governing equation of sandwich beam resting on Pasternak foundation. The GDQ approach was developed by Shu (2000) [A brief review of GDQ method is given in Appendix]. In harmonic vibration analysis of Timoshenko beam, the displacements can be expressed as

$$\begin{aligned}
\bar{U}(x,\tau)&=u(x)e^{-i\omega\tau}\\
\bar{W}(x,\tau)&=w(x)e^{-i\omega\tau}\\
\bar{\psi}(x,\tau)&=\psi(x)e^{-i\omega\tau}
\end{aligned} \quad (49)$$

where $i=\sqrt{-1}$ and $\omega^*=\omega L\sqrt{I_{10}/A_{110}}$ are the dimensionless natural frequency. It should be mentioned that ω is the natural frequency of the structure. By substituting Eq. (49) into Eqs. (41)-(43) and then applying the GDQ rule, the following relations are obtained

$$\begin{aligned}
&a_{11}\sum_{j=1}^{N}c_{ij}^2u_j+b_{11}\sum_{j=1}^{N}c_{ij}^2\psi_j=-\bar{I}_1\omega^{*2}u_i-\bar{I}_2\omega^{*2}\psi_i\\
&k^*a_{55}\left(\sum_{j=1}^{N}c_{ij}^2w_j+\sum_{j=1}^{N}c_{ij}^1\psi_j\right)-k_w w_i+k_s\sum_{j=1}^{N}c_{ij}^2w_j=-\bar{I}_1\omega^{*2}w_i\\
&b_{11}\sum_{j=1}^{N}c_{ij}^2u_j+d_{11}\sum_{j=1}^{N}c_{ij}^2\psi_j-k^*\bar{\eta}a_{55}\left(\sum_{j=1}^{N}c_{ij}^1w_j+\bar{\eta}\psi_i\right)=-\bar{I}_2\omega^{*2}u_i-\bar{I}_3\omega^{*2}\psi_i
\end{aligned} \quad (50)$$

The associated boundary conditions can be handled in the same way. For example, the dimensionless boundary condition of clamped–hinged (C-H) supported beams is

$$\begin{aligned}
&u_1=w_1=\psi_1=0 \quad at \quad \xi=0\\
&\begin{cases}
u_N=w_N=0\\
Mx=b_{11}\sum_{j=1}^{N}c_{Nj}^1u_j+d_{11}\sum_{j=1}^{N}c_{Nj}^1\psi_j=0 \quad at \quad \xi=1
\end{cases}
\end{aligned} \quad (51)$$

Implementing the boundary conditions into equation (50) leads to the following system of algebraic

$$\begin{bmatrix}[S_{bb}] & [S_{bd}]\\ [S_{db}] & [S_{dd}]\end{bmatrix}\begin{Bmatrix}\{U_b\}\\ \{U_d\}\end{Bmatrix}=\omega^2\begin{bmatrix}[0] & [0]\\ [0] & [\bar{I}_i]\end{bmatrix}\begin{Bmatrix}\{U_b\}\\ \{U_d\}\end{Bmatrix} \quad (52)$$

where $\{U_d\}$ and $\{U_b\}$ are as follows

$$\begin{aligned}
\{U_b\}&=\{\{u_b\} \quad \{w_b\} \quad \{\psi_b\}\}^T,\\
\{U_d\}&=\{\{u_d\} \quad \{w_d\} \quad \{\psi_d\}\}^T
\end{aligned} \quad (53)$$

In the above relation, subscripts "b" and "d" refer to the points at the boundary and in the interior domain, respectively. $[\bar{I}_i]$ is dimensionless inertia terms matrices. Eliminating the boundary degrees of freedom, this equation becomes

$$([S]-\omega^2[\bar{I}_i])\{U_d\}=\{0\} \quad (54)$$

where

$$[S]=[S_{dd}]-[S_{db}][S_{bb}]^{-1}[S_{bd}] \quad (55)$$

The natural frequency parameters of the considered FG-sandwich beam can be determined by solving the standard eigenvalue problem.

6. Numerical results and discussion

6.1 Verification

In this section, the accuracy of the method in evaluating the non-dimensional natural frequencies of the beams are investigated. The dimensionless fundamental natural frequency and critical buckling load obtained in the present analysis are compared in Tables 3 and 4 with the results given by Yas and Samadi (2012) by employing Timoshenko beam theory and the generalized differential quadrature method and those by Wattanasakulpong and Ungbhakorn (2013) who used the third order shear deformation theory. As can be observed, our results agree well with the published results.

Table 3 Dimensionless fundamental natural frequency of FG-CNTRC beams (L/h=15, V^*_{CNT}=0.12)

	H-H beam			C-C beam		
	UD	O	X	UD	O	X
Yas and Samadi (2012)	0.9753	0.7527	1.1150	1.5085	1.3180	1.6000
Wattanasakulpong and Ungbhakorn (2013)	0.9745	0.7453	1.1152	-	-	-
Present	0.9750	0.7523	1.1152	1.5087	1.3177	1.6009

Table 4 Comparison of fundamental frequency parameters of clamped-clamped FG-CNTR beams reinforced by aligned CNTs and rested on Pasternak foundation (L/h=15, V^*_{CNT}=0.12, K_w=0.1, K_s=0.02)

Type		ω_1^*	ω_2^*	ω_3^*
UD	Yas and Samadi (2012)	1.6038	3.2714	5.1779
	Present	1.5991	3.2594	5.1574
FG-Λ	Yas and Samadi (2012)	1.5096	3.1420	5.0216
	Present	1.5055	3.1308	5.0022
FG-O	Yas and Samadi (2012)	1.4282	3.0249	4.8750
	Present	1.4248	3.0150	4.8573
FG-X	Yas and Samadi (2012)	1.6895	3.3937	5.3264
	Present	1.6834	3.3802	5.3037

6.2 Benchmark results

In this section, we characterize the response of FG beam considering the effects of waviness, internal pores and graphene platelets (GPLs), Winkler foundation modulus, shear elastic foundation modulus and geometrical conditions. The non-dimensional natural frequency, Winkler and shearing layer elastic coefficients are assumed as follow

$$\Omega = \omega L^2 \sqrt{\frac{\rho^m A^*}{E^m I^*}} \tag{56}$$

$$k_w = \frac{K_w L^2}{A_{110}} \tag{57}$$

$$k_s = \frac{K_s}{A_{110}} \tag{58}$$

In which A_{110} and I_{10} are the values of A_{11} and I_1 of a homogeneous beam. A* and I* are the cross section and the moment of inertia of the cross section of the beam, respectively ρ_m and E_m are mechanical properties of CNTs.

The variation of natural frequencies in terms of the porosity coefficient and side-to-thickness ratio for Clamped-Clamped FG sandwich beams is plotted in Fig. 3. It can be seen from this figure that a porous nanocomposite sandwich beam has lower natural frequencies than a perfect beam (e_0=0). In other words, increasing porosity coefficient results in smaller natural frequencies due to the reduction in the bending rigidity of the sandwich beam. Therefore, for better understanding of mechanical behavior of nanocomposite beam, it is crucial to consider porosities inside the material of structure. It is also seen from this figure that with increasing side-to-thickness ratio, the frequencies increasing and for great amount of side-to-thickness ratio (L/h>15) the frequencies become almost constant.

The effect of CNT aspect ratio is depicted in Fig. 4. This figure illustrates frequency parameters of Clamped-Clamped sandwich beams for different amounts of V^*_{CN}, including 0.12, 0.17 and 0.28. This figure reveals that increasing of CNT aspect ratio (AR) leads to a little increases frequency parameters.

The influence of weight fraction on vibration frequency of the nanocomposite FG beams with respect to the Pasternak parameter of elastic medium is presented in Fig. 5. It is observed that increasing the weight fraction of GPLs results in larger values of vibration frequency which highlights their reinforcing effect on the structure. It is also seen that with increasing the shearing layer elastic coefficient the non-dimensional natural frequency of sandwich structure sharply increasing.

The effects of variation of the Winkler elastic coefficient on the non-dimensional natural frequency parameters of FG sandwich beam and for different values of porosity coefficient are shown in Fig. 6. It is clear that in all cases, with increasing the elastic coefficients of the foundation, the frequency parameters increase. It should be noted that higher values of Winkler and Pasternak foundation constants yield increase in bending rigidity and natural frequency of the structure. However, surrounding shear layer (K_s) has a continuous interaction with the sandwich beam and its effect on the vibration frequency is more sensible than Winkler layer.

To make clear the effect of boundary condition on the natural frequencies of FG sandwich beam, the natural frequencies of the structure with C-C, C-F and C-H boundary conditions are compared with each other in Fig. 7.

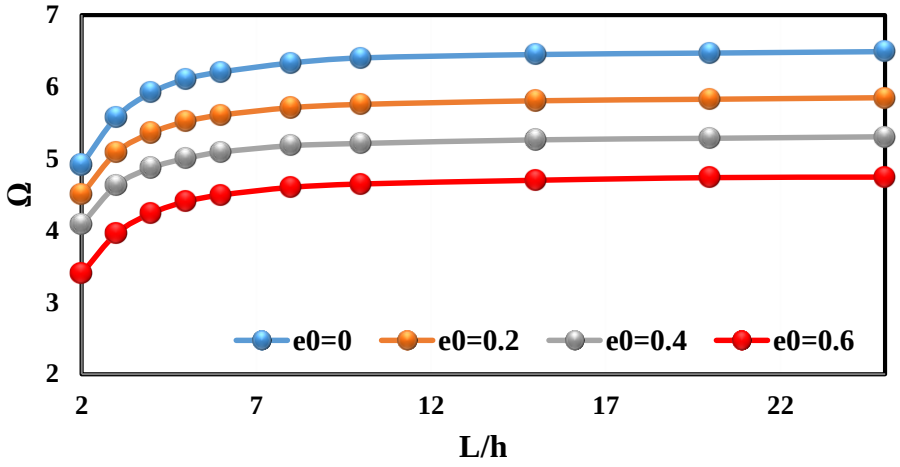

Fig. 3 Natural frequency of C-C Uniform GPLs-reinforcement sandwich beam versus side-to-thickness ratio (V_{CN}^{*} =0.28, AR=1000, K_s=K_w=100, GPL weight fraction, 0.1 wt.%)

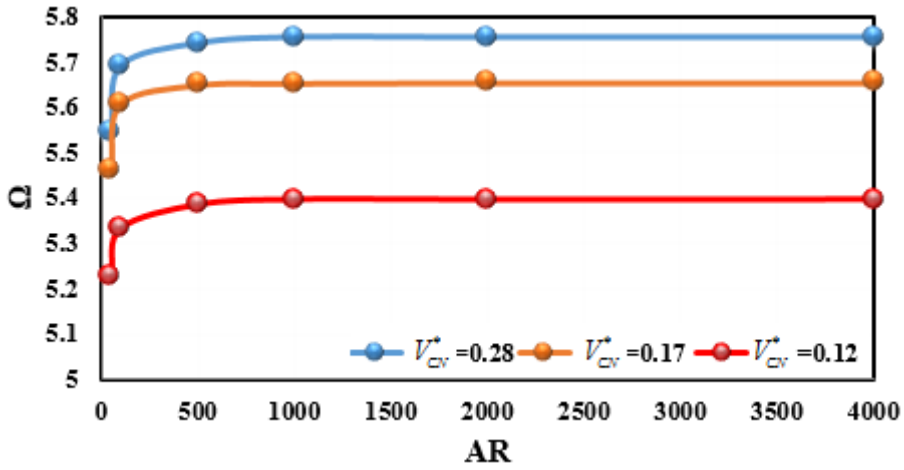

Fig. 4 Natural frequency of C-C Uniform GPLs-reinforcement sandwich beam versus CNT aspect ratio (AR) for different amount of V_{CN}^{*} (K_s=K_w=100, GPL weight fraction, 0.1 wt.%, e_0=0.2, L/h=10)

The natural frequency of C-C FG sandwich beam is significantly higher than those of Sandwich beam with C-F and C-H boundary conditions. As expected, increasing the degrees of freedom in the edges, decreases the natural frequencies.

The combined effects of porosity distribution and GPL distribution pattern on the fundamental frequency are investigated in Fig. 8 in which the fundamental natural frequency at various GPL weight fractions is presented. Symmetric GPL pattern A is proved to be the best dispersion method, followed by the uniform pattern C which is slightly better than the asymmetric pattern B. Results indicate that sandwich beam with non-uniform symmetric porosity distribution 1 and symmetric GPL pattern A have the largest fundamental frequencies, i.e., the highest effective stiffness under the same GPL weight fraction, suggesting that a nanocomposite beam in which both internal pores and nanofillers are symmetrically distributed can offer the best structural performance. It should be noted this tendency has been seen in other types of boundary conditions but for the sake of brevity, they are not reported here.

7. Conclusions

In this research work, free vibration of continuous grading FG beams on a two-parameter elastic foundation is investigated. The elastic foundation is considered as a Pasternak model with adding a shear layer to the Winkler model.

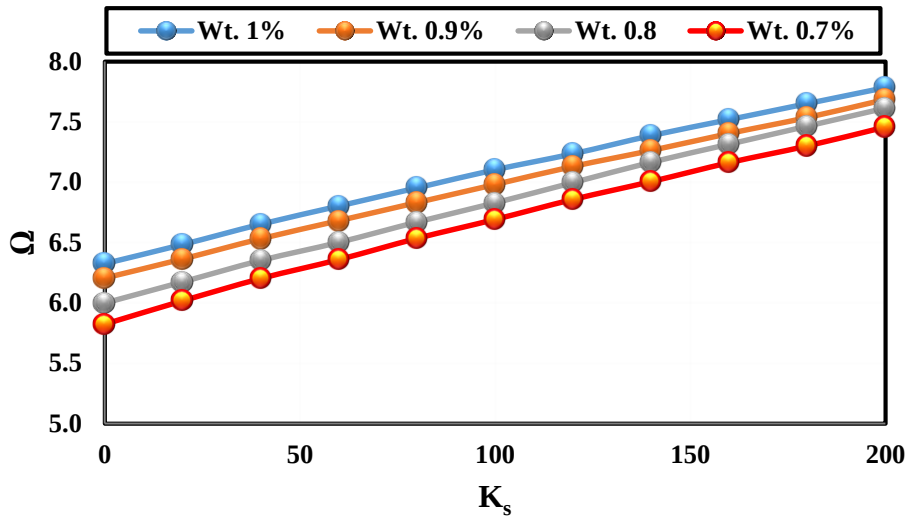

Fig. 5 The influence of shear elastic coefficient on natural frequency of C-C Uniform GPLs-reinforcement sandwich beam for different GPL weight fraction (K_w=100, AR=1000, L/h=10, e_0=0.2,$V_{CN}^{*}=0.28$)

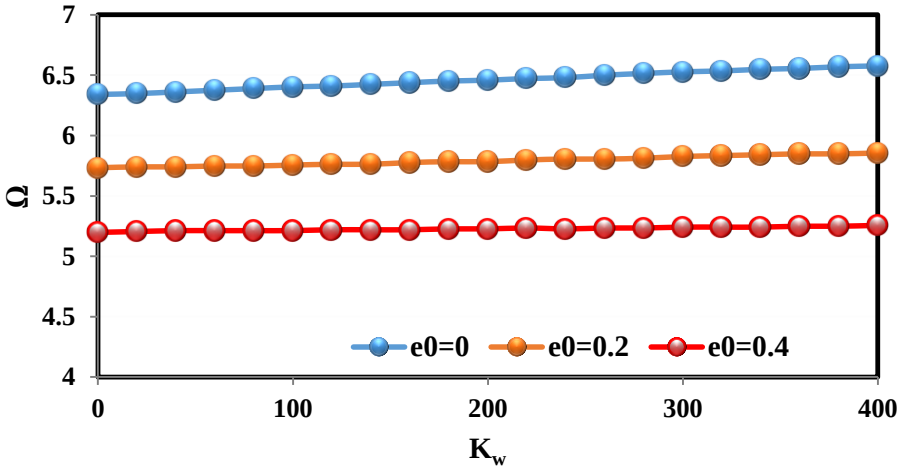

Fig. 6 The influence of Winkler elastic coefficient on natural frequency of C-C Uniform GPLs-reinforcement sandwich beam for different GPL weight fraction (K_s=100, AR=1000, L/h=10, e_0=0.2, $V_{CN}^{*}=0.28$)

The aim of this study is to fill this apparent gap in this area by investigating the effects of CNTs waviness and aspect ratio, porosity coefficient, porosity distribution, graphene platelets (GPLs) distribution, Winkler foundation modulus, shear elastic foundation modulus and geometrical conditions on the vibrational behavior of the sandwich structure. The distributions of CNTs are considered functionally graded (FG) or uniform along the thickness of upper and bottom layers of the sandwich beam and their mechanical properties are estimated by an extended rule of mixture. In this study, the classical theory concerning the mechanical efficiency of a matrix embedding finite length fibers has been modified by introducing the tube-to-tube random contact, which explicitly accounts for the progressive reduction of the tubes' effective aspect ratio as the filler content increases. The core of structure is porous and the internal pores and graphene platelets (GPLs) are distributed in the matrix of core either uniformly or non-uniformly according to three different patterns. From this study some conclusions can be made as following:

- It is observed that increasing of CNT aspect ratio (AR) leads to a little increases frequency parameters.
- Results reveal that increasing the weight fraction of GPLs results in larger values of vibration

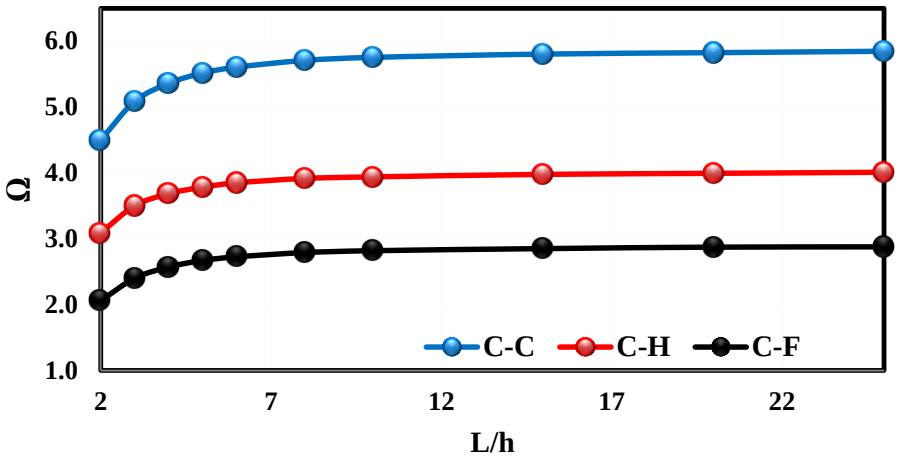

Fig. 7 The influence of different types of boundary conditions on natural frequency of Uniform GPLs-reinforcement sandwich beam (K_s=K_w=100, GPL weight fraction, 0.1 wt.%, AR=1000, L/h=10,$V_{CN}^{*}=0.28$, e_0=0.2)

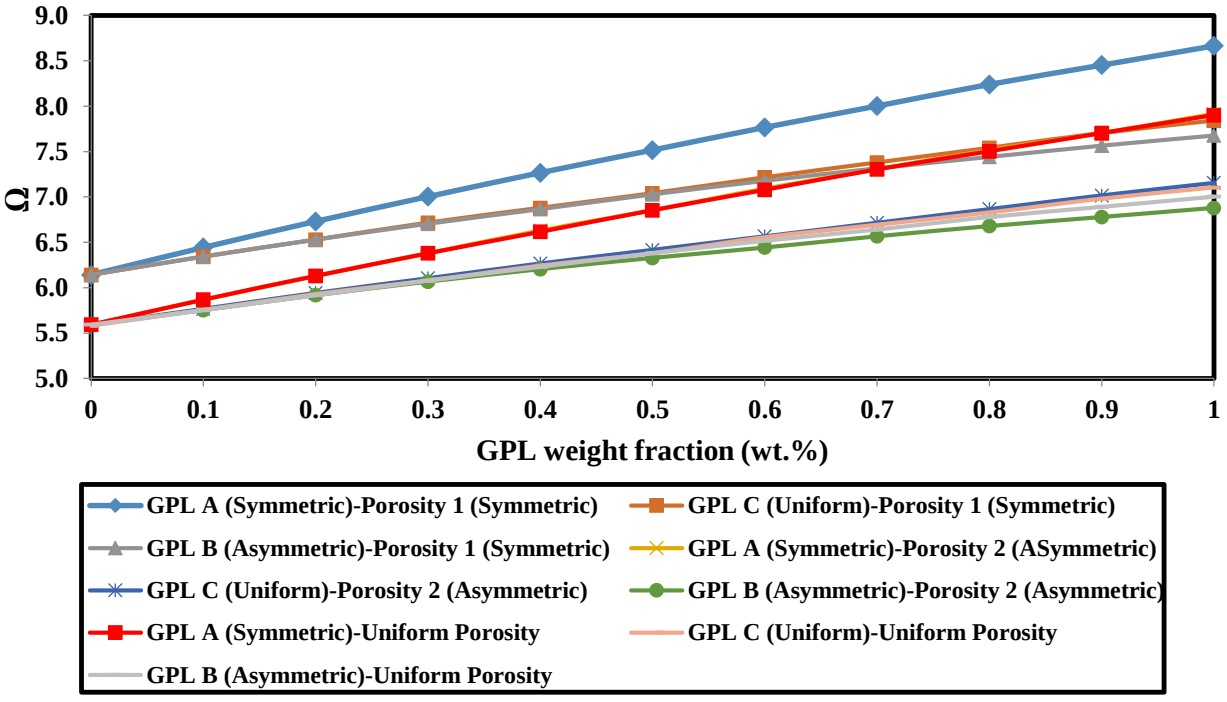

Fig. 8 The influence of GPL on natural frequency of GPLs-reinforcement sandwich beam (K_s=K_w=100, AR=1000, L/h=10,$V_{CN}^{*}=0.28$, e_0=0.2)

frequency which highlights their reinforcing effect on the structure.

- It should be noted that higher values of Winkler and Pasternak foundation constants yield increase in bending rigidity and natural frequency of the structure. However, surrounding shear layer (K_s) has a continuous interaction with the sandwich beam and its effect on the vibration frequency is more sensible than Winkler layer.
- The natural frequency of C-C FG sandwich beam is significantly higher than those of Sandwich beam with C-F and C-H boundary conditions. As

expected, increasing the degrees of freedom in the edges, decreases the natural frequencies.

- It is shown that increasing porosity coefficient results in smaller natural frequencies due to the reduction in the bending rigidity of the sandwich beam.
- According to the results, Symmetric GPL pattern A is proved to be the best dispersion method, followed by the uniform pattern C which is slightly better than the asymmetric pattern B.

Acknowledgments

The research described in this paper, supported by the National Natural Science Foundation of China (No. 41877251).

References

Ahmed Houari, M.S., Bessaim, A., Bernard, F., Tounsi, A. and Mahmoud, S.R. (2018), "Buckling analysis of new quasi-3D FG nanobeams based on nonlocal strain gradient elasticity theory and variable length scale parameter", *Steel Compos. Struct*., **28**(1), 13-24. https://doi.org/10.12989/scs.2018.28.1.013.

Affdl Halpin, J.C. and Kardos, J.L. (1976), "The Halpin-Tsai equations: A review", *Polym. Eng. Sci*., **16**(5), 344-352. https://doi.org/10.1002/pen.760160512.

Arefi, M. (2015), "Elastic solution of a curved beam made of functionally graded materials with different cross sections', *Steel Compos. Struct*., **18**(3), 659-672. https://doi.org/10.12989/scs.2015.18.3.659.

Arioui, O., Belakhdar, K., Kaci, A. and Tounsi, A. (2018), "Thermal buckling of FGM beams having parabolic thickness variation and temperature dependent materials", *Steel Compos. Struct*., **27**(6), 777-788. https://doi.org/10.12989/scs.2018.27.6.777.

Bambaeechee, M. (2019), "Free vibration of AFG beams with elastic end restraints", *Steel Compos. Struct*., **33**(3), 403-432. https://doi.org/10.12989/scs.2019.33.3.403.

Barka, M., Benrahou, K.H., Bakora, A. and Tounsi, A. (2016), "Thermal post-buckling behavior of imperfect temperature-dependent sandwich FGM plates resting on Pasternak elastic foundation", *Steel Compos. Struct*., **22**(1), 91-112. https://doi.org/10.12989/scs.2016.22.1.091.

Bouguenina, O., Belakhdar, K., Tounsi, A. and Bedia, E.A.A. (2015), "Numerical analysis of FGM plates with variable thickness subjected to thermal buckling", *Steel Compos. Struct*., **19**(3), 679-695. https://doi.org/10.12989/scs.2015.19.3.679.

Bennai, R., Ait Atmane, H. and Tounsi, A. (2015), "A new higher-order shear and normal deformation theory for functionally graded sandwich beams", *Steel Compos. Struct*., **19**(3), 521-546. https://doi.org/10.12989/scs.2015.19.3.521.

Bert, C.W. and Malik, M. (1996), "Differential quadrature method in computational mechanics: a review", *Appl. Mech. Rev.*, **49**, 1-27. https://doi.org/10.1115/1.3101882.

Bouchafa, A., Bouiadjra, M.B., Houari, M.S.A. and Tounsi, A. (2015), "Thermal stresses and deflections of functionally graded sandwich plates using a new refined hyperbolic shear deformation theory", *Steel Compos. Struct*., **18**(6), 1493-1515. https://doi.org/10.12989/scs.2015.18.6.1493.

Celep, Z. (1980), "Stability of a beam on an elastic foundation subjected to a nonconservative load", *J. Appl. Mech*., **47**(1), 116–120. https://doi.org/10.1115/1.3153587.

Chen, C.S., Liu, F.H. and Chen, W.R. (2017), "vibration and stability of initially stressed sandwich plates with FGM face sheets in thermal environments", *Steel Compos. Struct*., **23**(3), 251-261. https://doi.org/10.12989/scs.2017.23.3.251.

Du, H., Liew, K.M. and Lim, M.K. (1996), "Generalized differential quadrature method for buckling analysis", *J. Eng. Mech*., **122**(2), 95–100. https://doi.org/10.1061/(ASCE)0733-9399(1996)122:2.

Ebrahimi, S., Zahrai, S.M. and Mirghaderi, S.R. (2019), "Numerical study on force transfer mechanism in through gusset plates of SCBFs with HSS columns & beams", *Steel Compos. Struct*., **31**(6), 541-558. https://doi.org/10.12989/scs.2019.31.6.541.

Finot, M. and Suresh, S. (1996), "Small and large deformation of thick and thin-film multilayers: effect of layer geometry, plasticity and compositional gradients", *J. Mech. Phys. Solids*, **44**(5), 683-721. https://doi.org/10.1016/0022-5096(96)84548-0.

Hadji, L., Daouadji, T.H., Tounsi, A. and Bedia, E.A. (2014), "A higher order shear deformation theory for static and free vibration of FGM beam", *Steel Compos. Struct*., **16**(5), 507-519. https://doi.org/10.12989/scs.2014.16.5.507.

Halpin, J.C. and Tsai, S.W. (1969), "Effects of environmental factors on composite materials", *AFML-TR*-67-423.

Hauger, W. and Vetter, K. (1976), "Influence of an elastic foundation on the stability of a tangentially loaded column", *J. Sound Vib*., **47**(2), 296–299. https://doi.org/10.1016/10.1016/0022-460x(76)90726-4.

Karami, G., Malekzadeh, P. and Shahpari, S. (2003), "A DQEM for vibration of deformable non-uniform beams with general boundary conditions", *Eng. Struct*., **25**, 1169-1178. https://doi.org/10.1016/S0141-0296(03)00065-8.

Kitipornchai, S., Chen, D. and Yang, J. (2017), "Free vibration and elastic buckling of functionally graded porous beams reinforced by graphene platelets", *Mater. Design*, **116**, 656-665. https://doi.org/10.1016/j.matdes.2016.12.061.

Koizumi, M. (1993), "The concept of FGM", *Ceram. Trans. Funct. Grad. Mater*., **34**, 3-10.

Lee, S.Y., Yang, C.C. (1994), "Nonconservative instability of non-uniform beams resting on an elastic foundation", *J. Sound Vib*., **169**, 433–444. https://doi.org/10.1006/jsvi.1994.1027.

Lai, B., Richard, J.Y. and Xiong, M. (2019), "Experimental and analytical investigation of composite columns made of high strength steel and high strength concrete", *Steel Compos. Struct*., **33**(1), 67-79. https://doi.org/10.12989/scs.2019.33.1.067.

Leissa, A.W., McGee, O.G. and Huang, C.S. (1993), "Vibrations of sectorial plates having corner stress singularities", *J. Appl. Mech. Transactions of the ASME*, **60**(1), 134-140. https://doi.org/10.1115/1.2900735.

Liu, R. and Wang, L. (2015), "Thermal vibration of a single-walled carbon nanotube predicted by semiquantum molecular dynamics", *Physical Chemistry Chemical Physics*, 7. https://doi.org/10.1039/C4CP05495D.

Li, X., Zhou, X., Liu J. and Wang, X. (2019), "Shear behavior of short square tubed steel reinforced concrete columns with high-strength concrete", *Steel Compos. Struct*., **32**(3), 411-422. https://doi.org/10.12989/scs.2019.32.3.411.

Mahmoud, A.A., Awadalla, R. and Nassar, N.M. (2011), "Free vibration of non-uniform column using DQM", *Mech. Res. Commun.*, **38**, 443-448. https://doi.org/10.1016/j.mechrescom.2011.05.015.

Marin, M. (2010), "Lagrange identity method for microstretch thermoelastic materials", *J. Math. Anal. Appl*., **363**(1), 275-286`. https://doi.org/10.1016/j.jmaa.2009.08.045.

Marin, M. (2010), "Some estimates on vibrations in thermoelasticity of dipolar bodies", *J. Vib. Control*, **16**(1), 33-47. https://doi.org/10.1177/1077546309103419.

Marin, M., Agarwal, R.P. and Mahmoud, S.R. (2013), "Nonsimple material problems addressed by the Lagrange's identity", *Bound.*

Value Probl, **2013**(1-14). https://doi.org/10.1186/1687-2770-2013-135.

Marin, M. and Nicaise, S. (2016), "Existence and stability results for thermoelastic dipolar bodies with double porosity", *Continuum Mech. Thermodyn.*, **28**(6), 1645-1657. https://doi.org/10.1007/s00161-016-0503-4.

Marin, M., Ellahi, R. and Adina, C. (2017), "On solutions of Saint-Venant's problem for elastic dipolar bodies with voids", *Carpathian J. Math.*, **33**(2), 219-232.

Marin, M., Craciun, E.M. and Pop, N. (2016), "Considerations on mixed initial boundary value problems for micropolar porous bodies", *Dyn. Syst. Appl.*, **25**(1), 175-195.

Martone, A., Faiella, G., Antonucci, V., Giordano, M. and Zarrelli, M. (2011), "The effect of the aspect ratio of carbon nanotubes on their effective reinforcement modulus in an epoxy matrix", *Compos. Sci. Technol.*, **71**(8), 1117-1123. https://doi.org/10.1016/j.compscitech.2011.04.002.

Mirjavadi, S.S., Afshari, B.M., Shafiei, N., Hamouda, A.M.S. and Kazemi, M. (2017), "Thermal vibration of two-dimensional functionally graded (2D-FG) porous Timoshenko nanobeams", *Steel Compos. Struct.*, **25**(4), 415-426. https://doi.org/10.12989/scs.2017.25.4.415.

Montazeri, A., Javadpour, J., Khavandi, A., Tcharkhtchi, A. and Mohajeri, A. (2010), "Mechanical properties of multi-walled carbon nanotube/epoxy composites", *Mater. Des.*, **31**, 4202-4208. https://doi.org/10.1016/j.matdes.2010.04.018.

Moradi-Dastjerdi, R. and Momeni-Khabisi, H. (2016), "Dynamic analysis of functionally graded nanocomposite plates reinforced by wavy carbon nanotube", *Steel Compos. Struct.*, **22**(2). https://doi.org/10.12989/scs.2016.22.2.277.

Moradi-Dastjerdi, R., Foroutan, M. and Pourasghar, A. (2013), "Dynamic analysis of functionally graded nanocomposite cylinders reinforced by carbon nanotube by a mesh-free method", *Mater. Des.*, **44**, 256-266.

Nguyen, D.K. and Tran, T.T. (2018), "Free vibration of tapered BFGM beams using an efficient shear deformable finite element model", *Steel Compos. Struct.*, **29**(3), 363-377. https://doi.org/10.12989/scs.2018.29.3.363.

Nguyen, X.H., Le, D.D. and Nguyen, Q.H. (2019), "Static behavior of novel RCS through-column-type joint: Experimental and numerical study", *Steel Compos. Struct.*, **32**(1), 111-126. https://doi.org/10.12989/scs.2019.32.1.111.

Park, W.T., Han, S.C., Jung, W.Y. and Lee, W.H. (2016), "Dynamic instability analysis for S-FGM plates embedded in Pasternak elastic medium using the modified couple stress theory", *Steel Compos. Struct.*, **22**(6), 1239-1259. https://doi.org/10.12989/scs.2016.22.6.1239.

Pelletier Jacob, L. and Vel Senthil,S. (2006), "An exact solution for the steady state thermo elastic response of functionally graded orthotropic cylindrical shells", *Int. J. Solid Struct.*, **43**, 1131-1158. https://doi.org/10.1016/j.ijsolstr.2005.03.079.

Quan, J.R. and Chan, C.T. (1989), "New insights in solving distributed system equation by the quadrature methods", *Comput. Chem. Eng.*, **13**, 779-788. https://doi.org/10.1016/0098-1354(89)85051-3.

Sharma, A., Sharda, H.B. and Nath, Y. (2005a), "Stability and vibration of Mindlin sector plates: an analytical approach", *AIAA J.*, **43**(5), 1109-1116. https://doi.org/10.2514/1.4683.

Sharma, A., Sharda, H.B. and Nath, Y. (2005b), "Stability and vibration of thick laminated composite sector plates", *J. Sound Vib.*, **287**(1-2), 1-23. https://doi.org/10.1016/j.jsv.2004.10.030.

Shafiei, H. and Setoodeh, A.R. (2017), "Nonlinear free vibration and post-buckling of FG-CNTRC beams on nonlinear foundation", *Steel Compos. Struct.*, **24**(1), 65-77. https://doi.org/10.12989/scs.2017.24.1.065.

Shen H.S. (2009), "Nonlinear bending of functionally graded carbon nanotube reinforced composite plates in thermal environments", *Compos. Struct.*, **91**(1), 9-19.

Shen, H.S. and Zhang, C.L. (2010), "Thermal buckling and postbuckling behavior of functionally graded carbon nanotube-reinforced composite plates", *Mater. Des.*, **31**(7), 3403-3411.

Shu, C. and Du, H. (1997a), "Implementation of clamped and simply supported boundary conditions in the GDQ free vibration analysis of beams and plates", *Int. J. Solids. Struct.*, **34**, 819-835. https://doi.org/10.1016/S0020-7683(96)00057-1.

Shu, C. and Du, H. (1997b), "A generalized approach for implementing general boundary conditions in the GDQ free vibration analysis of plates", *Int. J. Solids. Struct.*, **34**, 837-846. https://doi.org/10.1016/S0020-7683(96)00056-X.

Shu, C. (2000), "Differential Quadrature and Its Application in Engineering", Springer, Berlin.

Smith, T.E. and Herrmann, G. (1972), "Stability of a beam on an elastic foundation subjected to a follower force", *J. Appl. Mech.*, **39**, 628–629. https://doi.org/10.1115/1.3422743.

Song, Y., Uy, B. and Wang, J. (2019), "Numerical analysis of stainless steel-concrete composite beam-to-column joints with bolted flush endplates", *Steel Compos. Struct.*, **33**(1), 143-162. https://doi.org/10.12989/scs.2019.33.1.143.

Sundararajan, C. (1974), "Stability of columns on elastic foundations subjected to conservative or nonconservative forces", *J. Sound Vib.*, **37**(1), 79-85. https://doi.org/10.1016/S0022-460X(74)80059-3.

Tahouneh, V. (2016), "Using an equivalent continuum model for 3D dynamic analysis of nanocomposite plates", *Steel Compos. Struct.*, **20**(3), 623-649. https://doi.org/10.12989/scs.2016.20.3.623.

Tahouneh, V. (2017), "The effect of carbon nanotubes agglomeration on vibrational response of thick functionally graded sandwich plates", *Steel Compos. Struct.*, **24**(6), 711-726. https://doi.org/10.12989/scs.2017.24.6.711.

Tornabene, F., Bacciocchi, M., Fantuzzi, N. and Reddy, J.N. (2018), "Multiscale Approach for Three-Phase CNT/Polymer/Fiber Laminated Nanocomposite Structures", *Polymer Composites*, In Press, DOI: 10.1002/pc.24520.

Tornabene, F., Fantuzzi, N., Ubertini, F. and Viola, E. (2015), "Strong formulation finite element method based on differential quadrature: A survey", *Appl. Mech. Rev.*, **67**(2), 1-55. https://doi.org/10.1115/1.4028859.

Tornabene, F., Fantuzzi, N. and Bacciocchi, M. (2019), "Refined shear deformation theories for laminated composite arches and beams with variable thickness: Natural frequency analysis", *Eng. Anal. Bound. Elem.*, **100**, 24-47. https://doi.org/10.1016/j.enganabound.2017.07.029.

Tornabene, F., Fantuzzi, N. and Bacciocchi, M. (2017), "Foam core composite sandwich plates and shells with variable stiffness: Effect of the curvilinear fiber path on the modal response", *J. Sandw. Struct. Mater.*, **21**(1), 320-365. https://doi.org/10.1177/1099636217693623.

Wagner, H.D., Lourie, O. and Feldman, Y. (1997), "Stress-induced fragmentation of multiwall carbon nanotubes in a polymer matrix", *Appl. Phys. Lett.*, **72**(2), 188-190. https://doi.org/10.1063/1.120680.

Wang, X. and Bert, C.W. (1993), "A new approach in applying differential quadrature to static and free vibrational analysis of beam and plates", *J. Sound Vib.*, **162**(3), 566-572. https://doi.org/10.1006/jsvi.1993.1143.

Wang, J. and Sun, Q. (2019), "Seismic behavior of Q690 circular HCFTST columns under constant axial loading and reversed cyclic lateral loading", *Steel Compos. Struct.*, **32**(2), 199-212. https://doi.org/10.12989/scs.2019.32.2.199.

Wattanasakulpong, and Ungbhakorn, V. (2013), "Analytical solutions for bending, buckling and vibration responses of carbon nanotube-reinforced composite beams resting on elastic foundation", *Comput. Mater. Sci.*, **71** 201-208.

Wu, C.P. and Liu, Y.C. (2016), "A state space meshless method for the 3D analysis of FGM axisymmetric circular plates", *Steel Compos. Struct.*, **22**(1), 161-182. https://doi.org/10.12989/scs.2016.22.1.161.

Xu, W., Wang, L. and Jiang, J. (2016), "Strain gradient finite element analysis on the vibration of double-layered graphene sheets", *Int. J. Comput. Method.*, **13**(3). https://doi.org/10.1142/S0219876216500110.

Yaghoobi, H., Valipour, M.S., Fereidoon, A. and Khoshnevisrad, P. (2014), "Analytical study on post-buckling and nonlinear free vibration analysis of FG beams resting on nonlinear elastic foundation under thermo-mechanical loadings using VIM", *Steel Compos. Struct.*, **17**(5), 753-776. https://doi.org/10.12989/scs.2014.17.5.753.

Yas, M. and Samadi, N. (2012), "Free vibrations and buckling analysis of carbon nanotube-reinforced composite Timoshenko beams on elastic foundation", *Int. J. Pressure Vessel. Piping*, **98**, 119-128.

Yeh, M.K., Tai, N.H. and Liu, J.H. (2006), "Mechanical behavior of phenolic-based composites reinforced with multi-walled carbon nanotubes", *Carbon*, **44**(1), 1-9. https://doi.org/10.1016/j.carbon.2005.07.005.

Yusheng, F. and Bert, C.W. (1992), "Application of quadrature method to flexural vibration analysis of a geometrically nonlinear beam", *J. Nonlinear Dynam.*, **3**, 13-18.

Zhang, Y. and Wang, L. (2018), "Thermally stimulated nonlinear vibration of rectangular single-layered black phosphorus", *J. Appl. Phys.*, **124**(13), 10.1063/1.5047584. https://doi.org/10.1063/1.5047584.

Zhu, X.H. and Meng, Z.Y. (1995), "Operational principle fabrication and displacement characteristics of a functionally gradient piezoelectricceramic actuator", *Sens. Actuators*, **48**(3), 169-176. https://doi.org/10.1016/0924-4247(95)00996-5.

CC

Appendix

In Generalized Differential Quadrature Method (GDQM), the *n*th order partial derivative of a continuous function $f(x,z)$ with respect to x at a given point x_i can be approximated as a linear summation of weighted function values at all the discrete points in the domain of *x*, that is

$$\frac{\partial^n f_{(x_i,z)}}{\partial x^n} = \sum_{k=1}^{N} c_{ik}^n f_{(x_{ik},z)} \quad (i=1,2,...,N, n=1,2,...,N-1) \tag{1}$$

Where *N* is the number of sampling points and c_{ij}^n is the x^i dependent weight coefficient. To determine the weighting coefficients c_{ij}^n, the Lagrange interpolation basic functions are used as the test functions, and explicit formulas for computing these weighting coefficients can be obtained as (Bert and Malik 1996)

$$c_{ij}^{(1)} = \frac{M^{(1)}(x_i)}{(x_i - x_j)M^{(1)}(x_j)}, i, j = 1,2,...,N, i \neq j \tag{2}$$

where

$$M^{(1)}(x_i) = \prod_{j=1, i\neq j}^{N} (x_i - x_j) \tag{3}$$

and for higher order derivatives, one can use the following relations iteratively

$$c_{ij}^{(n)} = n(c_{ii}^{(n-1)} c_{ij}^{1} - \frac{c_{ij}^{(n-1)}}{(x_i - x_j)}), \quad i, j = 1,2,...,N, \tag{4}$$

$$i \neq j, n = 2,3,...,N-1$$

$$c_{ii}^{(n)} = -\sum_{j=1, i\neq j}^{N} c_{ij}^{(n)} \quad i = 1,2,...,N, \quad n = 1,2,...,N-1 \tag{5}$$

A simple and natural choice of the grid distribution is the uniform grid-spacing rule. However, it was found that nonuniform grid-spacing yields result with better accuracy. Hence, in this work, the Chebyshev-Gauss-Lobatto quadrature points are used

$$x_i = \frac{1}{2}(1 - \cos(\frac{i-1}{N-1}\pi)) \quad i = 1,2,...,N \tag{6}$$